Penerbit Akademia Baru

Malaysian Journal on Composites Science and Manufacturing

Journal homepage:
https://www.akademiabaru.com/submit/index.php/mjcsm/
ISSN: 2716-6945

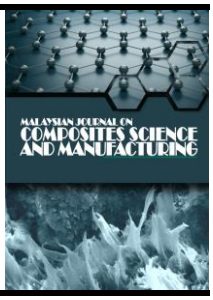

Numerical Investigation on the Aerodynamic Characteristics of a Wing for Various Flow and Geometrical Parameters

Open Access

Md. Saifi Bin Islam[1], Muhammad Faiz Ahmed[1*], Abdullah Al Saad[1]

[1] Department of Mechanical Engineering, Khulna University of Engineering & Technology, Khulna-9203, Bangladesh

ARTICLE INFO

Article history:
Received 10 September 2023
Received in revised form 2 November 2023
Accepted 22 November 2023
Available online 30 November 2023

ABSTRACT

The wing is a critical component of an aircraft, responsible for generating the lift force necessary for flight. The aerodynamic behavior of a wing is complex and is influenced by factors such as air speed, angle of attack, wing shape, twist angle, and turbulence. This research investigates the performance of NACA 4412 and NACA 4418 airfoils using 2D CFD, covering a range of angle-of-attack values from -5 to 20 degrees. The superior performing airfoil, NACA 4412, was selected for wing geometry which outperforms NACA 4418 in terms of lower drag and higher lift coefficient at both low and high Reynolds numbers. Then 3D CFD analysis was employed to study how wings perform at different Reynolds numbers and the optimal twist angle for the wing was determined, focusing on a steady-state analysis. The Reynolds number range which corresponds to the flow velocity range, is used in this numerical study for 3D wings. The result shows that as the Reynolds number increases, the wing's lift coefficient proportionally rises, owing to higher flow velocities. However, this increase in Reynolds number also results in a higher drag coefficient due to a rise in turbulence. The investigation reveals the existence of an optimum twist angle for the wing, which maximizes the lift-to-drag coefficient ratio, thus enhancing overall aerodynamic performance.

Keywords:
Airfoil, Wing, Angle of Attack, Twist Angle, Computational Fluid Dynamics (CFD), Reynolds Number, Lift Coefficient, Drag Coefficient

1. Introduction

The design of an aircraft's wings has a direct impact on its aerodynamic effectiveness and stability, making it a key part of the aviation industry. A stable and functional wing design must take into account several complex factors, such as the wing's size, shape, angle of attack, and airfoil profile. Computational fluid dynamics (CFD) based numerical simulations have developed into a

* *Corresponding author.*
E-mail address: faiz.140509@gmail.com (Muhammad Faiz Ahmed)
E-mail of co-authors: saifiislam75@gmail.com, abdullahsaad283@gmail.com

https://doi.org/10.37934/mjcsm.12.1.1330

useful tool for forecasting the aerodynamic behavior of wings and improving their design. Computational tools have advanced airfoil and wing design, focusing on aerodynamic performance objectives like lift-to-drag ratios and Mach numbers. This drive for enhanced lift at higher speeds with reduced drag has led to knowledge bases for aerodynamic design, involving geometric, mechanical, and fluid dynamic modeling using powerful analytical software [1].

The forces and moments required for continuous airflow are studied in the branch of mechanics known as aerodynamics. Lift is the term for the aerodynamic force acting perpendicular to the direction of flight, and drag, often known as the propulsive force, is the term for the force acting in the direction of flight. These pressures are influenced by the relative wind, often known as the flow velocity far in front of the object. The way air interacts with a solid mass moving through it, like an airplane wing, can lead to aerodynamic issues. The ideal airfoil forms have attracted the attention of aerodynamics experts [2].

The National Advisory Committee for Aeronautics, or NACA, produced the first in-depth analysis of airfoil designs and performances. The three most critical characteristics of an airfoil's shape are chord, camber, and thickness [3]. Along with drag, pressure distribution, and moment about the aerodynamic center, the lift is one of the performance aspects of cataloged airfoils that is frequently included. These variables have been measured in wind tunnels, and their values have also been determined using mathematical theory calculations or by using computer models with CFD simulation tools [2].

Different sizes and shapes of aircraft wings are available, each with a particular function in mind. The linear wing, which is simple to produce, is the most popular kind of wing. This kind of wing is less effective at fast speeds and produces more drag. On the other hand, a swept-wing has a wing that is angled rearward, lowering drag and raising speed. This wing is perfect for high-speed flight and is frequently used on supersonic airplanes. The delta wing is a different kind of wing that has a triangular shape and offers high lift and minimal drag. Fighter planes and other high-performance aircraft use this kind of wing [4]. Aircraft efficiency hinges on wings primarily responsible for generating lift, allowing takeoff, flight, and maneuvering. Beyond lift, wings enhance speed, reduce noise, and improve fuel economy. They aid control and stability, especially during takeoff and landing, and can carry external loads like fuel tanks and weaponry. Additionally, wings harness wind energy. Unmanned aerial vehicles (UAVs) rely on wings for autonomous flight. Wings play a crucial role in aircraft and flying vehicle performance and safety [6].

Aerodynamics of flapping airfoils in tandem, low Reynolds number (N) research, and computational studies employing LES are all current areas of study. Numerous biological systems and power extraction technologies use oscillating airfoils. Airfoils' pitching and plummeting motion can provide lift, making it possible to use them as a propulsion device. The computational fluid dynamics (CFD) method is used in the current study to analyze a flapping flight mechanism. There is potential for research in understanding topics like rotor dynamics and bio-inspired flows, which requires understanding the kinematics of oscillating airfoils. Although unstable airfoils have received substantial study, newer and more complicated kinematics remain mostly unexplored. The implementation of a gradient-based technique in the current work expands on earlier research on the NACA0012-IK30 airfoil by looking for the leading-edge pitching amplitude that maximizes propulsion power [7].

In 2017, Cayiroglu and Kilic [8] conducted a computational study on optimizing wing aerodynamics using the genetic algorithm and Ansys, where the aerodynamic study of a private jet's wings was performed. The best wing was identified in that study as having the lowest center of pressure distance and the maximum lift/drag ratio [8]. Using ANSYS Fluent, Ives et al. [9] created and verified a simulation model of the external flow around the NACA 2412 in 2018. That model then be

used to generate data for a high velocity case, which is the practical velocity for commercial aircraft (272.1 m/s, Mach = 0.8). Their research focused on an aspect that has both an endless (2D) and a finite (3D) aspect ratio [9].

Compared to earlier studies employing flat plate geometries or symmetric NACA airfoils, simulations are now carried out using a modern cambered airfoil made for use in low Re situations. By Zilstra, A. and Johnson, D.A., in 2023. At a moderate Re of 4.1104 and 1°, 5°, and 7° angles of attack (AOAs), the cambered SD 7037 airfoil is simulated using wall-resolved large eddy simulation (LES), and the results are validated against experimental data. The location of the laminar separated bubble (LSB), which develops during the natural BL transition phase, is accurately predicted by pressure and skin friction coefficient simulations [10].

This study uses CFD simulations to do a numerical analysis of the aerodynamic performance of a wing. The study focuses on analyzing the performance parameters of different types of airfoils of a wing and selecting the optimal airfoil for wing design. Then, provides critical insights into how Reynolds numbers, twist angles, and airfoil choices influence wing aerodynamics, which can be invaluable for aircraft design and performance improvement.

1.1 Problem Description

Wing design is an important aspect of many engineering applications, especially in the aerospace and automotive sectors. A wing's efficiency and effectiveness depend on several factors, such as its size, twist angle, and shape. Physical experiments can be used to inform the design of a wing, but numerical simulations provide a more affordable and timely way to explore different design parameters.

The twist angle of a wing is one of the most important design factors influencing its aerodynamic performance. To design a more effective wing for a specific application, it is necessary to thoroughly examine the effect of twist angle on lift, drag, and other parameters. Therefore, a thorough numerical analysis of the aerodynamic properties of a wing is required, with a particular emphasis on the effect of twist angle [11].

2. Methodology

2.1 Governing Equations

The primary governing equations of fluid dynamics in computational fluid dynamics (CFD) are continuity, momentum, and energy.

2.1.1 Navier-Stokes Equation

The Navier-Stokes equation or the Equation of motion are other names for the general momentum equation. Navier-Stokes is the basic Equation for a viscous fluid. The following syntax can be used [12] to represent the Navier-Stokes equations for an incompressible three-dimensional flow:

$$\rho\left(\frac{dV}{dt}\right) = \rho g - \nabla p + \mu\nabla^2 V \tag{1}$$

For each dimension when the velocity is V (*u, v, and w*)

$$\rho(\frac{\partial u}{\partial t}) + u(\frac{\partial u}{\partial x}) + v(\frac{\partial u}{\partial y}) + w(\frac{\partial u}{\partial z}) = \rho g_x - (\frac{\partial p}{\partial x}) + \mu(\frac{\partial^2 u}{\partial x^2} + \frac{\partial^2 u}{\partial y^2} + \frac{\partial^2 u}{\partial z^2}) \tag{2}$$

$$(\frac{\partial v}{\partial t}) + u(\frac{\partial v}{\partial x}) + v(\frac{\partial v}{\partial y}) + w(\frac{\partial v}{\partial z}) = \rho g_y - (\frac{\partial p}{\partial y}) + \mu(\frac{\partial^2 v}{\partial x^2} + \frac{\partial^2 v}{\partial y^2} + \frac{\partial^2 v}{\partial z^2}) \quad (3)$$

$$(\frac{\partial w}{\partial t}) + u(\frac{\partial w}{\partial x}) + v(\frac{\partial w}{\partial y}) + w(\frac{\partial w}{\partial z}) = \rho g_z - (\frac{\partial p}{\partial z}) + \mu(\frac{\partial^2 w}{\partial x^2} + \frac{\partial^2 w}{\partial y^2} + \frac{\partial^2 w}{\partial z^2}) \quad (4)$$

Among these four Navier-Stokes equations, Eq. 1 is a time-dependent continuity equation for conservation of mass, and the other three are time-dependent conservation of momentum equations.

2.1.2 Continuity Equation

An equation that explains the motion of a preserved quantity is known as a continuity equation in physics. Continuity equations can be used to explain a variety of physical processes because, under the right circumstances, mass, energy, momentum, and other natural quantities all remain constant. Below is the continuity equation:

$$\frac{\partial \rho}{\partial t} + \frac{\partial u}{\partial x} + \frac{\partial v}{\partial y} + \frac{\partial w}{\partial z} = 0 \quad (5a)$$

For steady-state Two-Dimensional flow, the formula is as follows:

$$\frac{\partial u}{\partial x} + \frac{\partial v}{\partial y} = 0 \quad (5b)$$

2.2 Turbulence Model

Turbulence modeling is the process of using a model to predict the effects of turbulence. Most scenarios in the real world involve turbulent flows, including, but not limited to, the flow of blood through the body, air over an airplane wing, and spacecraft re-entry. There is no analytical theory that can predict how these turbulent flows would behave after decades of research. The equations regulating turbulent flows can only be solved directly in simple flow scenarios. For the bulk of turbulent flows in nature, CFD simulations use turbulent models to predict the development of turbulence. The statistical evolution of turbulent flows is predicted by these condensed constitutive equations for these turbulence models [13]. There are many turbulence models, among which K-epsilon (*k*-ε) and K-omega (*k*-ω) are most commonly used in CFD to simulate mean flow characteristics for turbulent flow. The k-epsilon model tends to show great results in the free stream region, and the k-omega model has good accuracy in the boundary layer region close to the wall. To combine the superior behavior of the *k*-ω model in the near-wall region with the robustness of the *k*-ε model, Menter introduced the SST (Shear Stress Transport) model, which interpolates between the two [14].

2.2.1 The SST K- ω turbulence model

The SST k-ω turbulence model is a two-equation eddy-viscosity model introduced by Menter in 1993, which has become very popular. Due to the use of a *k*-ω formulation in the inner regions of the boundary layer that permits direct utilization of the model down to the wall through the viscous sub-layer, the SST *k*-ω model can be used as a Low-Re turbulence model without the requirement for further damping functions. The SST formulation prevents the common *k*-ω problem by switching to

a *k*-ε behavior in the free stream, where the model is less susceptible to the characteristics of the inlet free-stream turbulence. In difficult pressure gradients and separate flow, the SST *k*-ω model consistently receives high marks from authors [14, 15].

2.3 Numerical Modeling

2.3.1 Model Analysis for Airfoils (2D)

2.3.1.1 Generating NACA 4412 & NACA 4418 Airfoils Profile

Creating an airfoil's coordinate points took theoretical and mathematical study. Many of these airfoils already have coordinates available in print or online. Also, a lot of tools and websites can now calculate the coordinate automatically after the user enters the required airfoil name or attributes.

Coordinates are gathered from the online profile generator for the NACA 4-digit airfoil series to correctly plot the profile of NACA 4412 shown in Figure 1and NACA 4418 shown in Figure 2. However, the data points are not yet prepared for usage in Fluent [16]. The airfoil data points are formatted in Microsoft Excel before being saved in the "Text (comma delimited)" format.

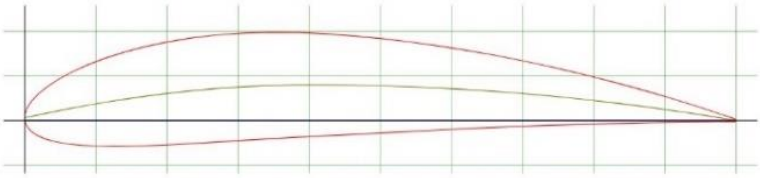

Fig.1. NACA 4412 Airfoil

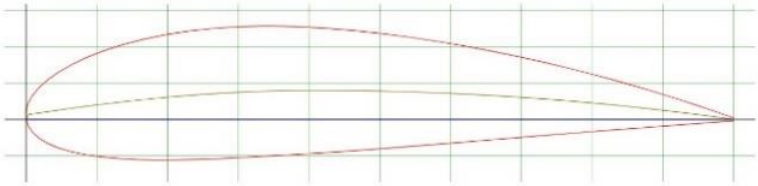

Fig.2. NACA 4418 Airfoil

2.3.1.2 Computational Domain for 2D Airfoil Analysis

NACA 4412 and NACA 4418 coordinates are first imported as Points into Solidworks to create the simulation's geometry. A curve is made using the points. A surface with a 0.1 m chord length is made to mimic the cross-section of NACA 4412 and NACA 4418. The C mesh is then sketched on the same plane as the airfoil to form a C mesh domain. The C mesh is then divided into four quadrants to aid in adjusting the surface mesh size. Figure 3 depicts the domain. The major semi-circular part is subtracted from the airfoil. The computational domain was 12.5C above the pressure surface, 12.5C below the leading edge of the airfoil, and 12.5C above the trailing edge. The radius of the C shape is also 12.5C. In Figure 3, the dimensions are in millimeters.

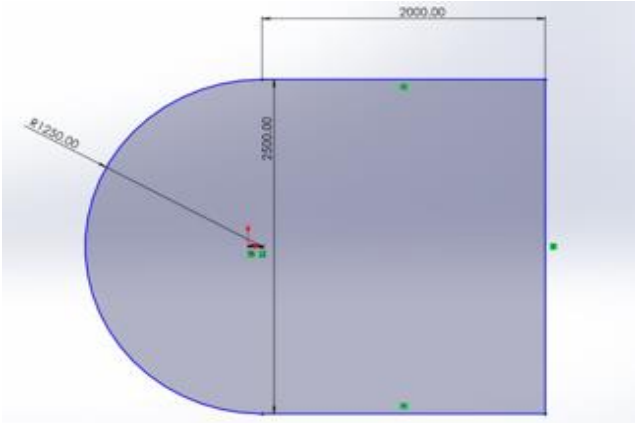

Fig.3. Computational domain for 2D airfoil analysis

2.3.1.3 Grid Generation and Wall Treatment for 2D Airfoils

The analysis region must be divided into numerous subregions to use the finite volume method. In Figure 4, these little areas are elements that are linked to one another at their nearby nodes. The generated elements' geometric properties impact the finite volume analysis's overall effectiveness and correctness. As a result, mesh creation is one of the most crucial steps in finite-volume modeling.

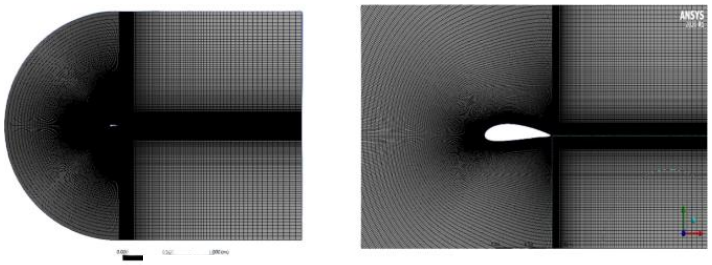

Fig.4. Mesh around NACA 4418 airfoil, (a) zoom-out view, and (b) zoom-in view

The element type for the meshing is linear hexahedral (C3D8R), which describes it as an 8-node linear brick with reduced integration and an hourglass control element. Mesh technology uses an organized approach. In the bonded area of adhesive and adherend, double biasing is applied in the meshing seed; 528000 total elements and 554187 total nodes make up the network.

For more accurate results, a dense or fine mesh must be used to compute the behavior of the viscous shear layer in the boundary layer. Contrarily, the thin mesh of the domain causes a rise in grid points and, eventually, CPU time. Adjusting the grid size near the wall will improve precision. By using structured mesh, this process, known as biasing, is considerably easier to carry out.

In this study, flow domains are subdivided into more manageable subdomains to study fluid flow. The governing equations are then discretized and solved within each of these sub-domains.

The quadrilaterals approach is used to create a C-type mesh that discretizes the airfoil's flow field—the 160000 elements in the C-type grid. The biasing approach is used to obtain accurate results in the near-wall or airfoil region. Also done is wall treatment. The steps are the same for NACA 4412 and NACA 4418.

2.3.1.4 Boundary Conditions for 2D Airfoils

In Figure 5, the final two vertical lines show the pressure outflow and the final two outer horizontal lines reflect the pressure far field. The circular arc section depicts the velocity entrance.

Concerning the Reynolds number, the upstream air velocity at the velocity inlet varies. The calculation of the velocity components is the outcome of each angle of attack. X and Y components of velocity are determined using the formulas x=u* cosα and y=u* sinα, respectively, where is the angle of attack in degrees. Turbulence intensity is taken into account at 1% for velocity inlet boundaries and 5% for pressure outlet boundaries. A turbulence viscosity ratio of 10 is also employed for a better approximation.

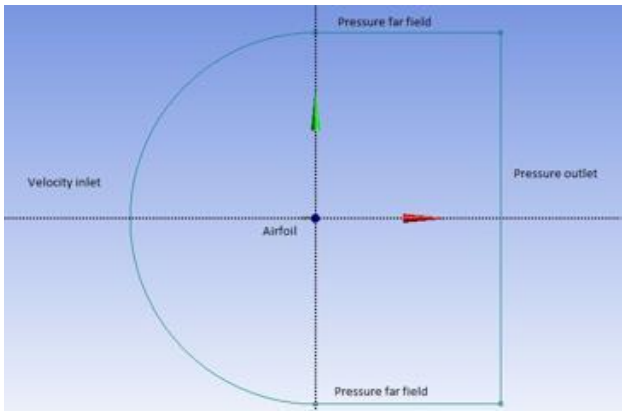

Fig.5. Boundary Condition for 2D airfoil analysis

2.3.2 Model Analysis for Wing (3D)

2.3.2.1 Generating Wing Geometry

The wing geometry shown in Figure 6 is created by Solidworks using NACA 4412 airfoil profile. The chord length of the root is 0.1m, and the tip is 40% of the root. Wing span is kept at 0.2m here. As the wing needs a twist angle, determining the optimal twist angle is one of the objectives of this research, so the twist angle varies from 2 to 20 degrees as shown in Figure 7.

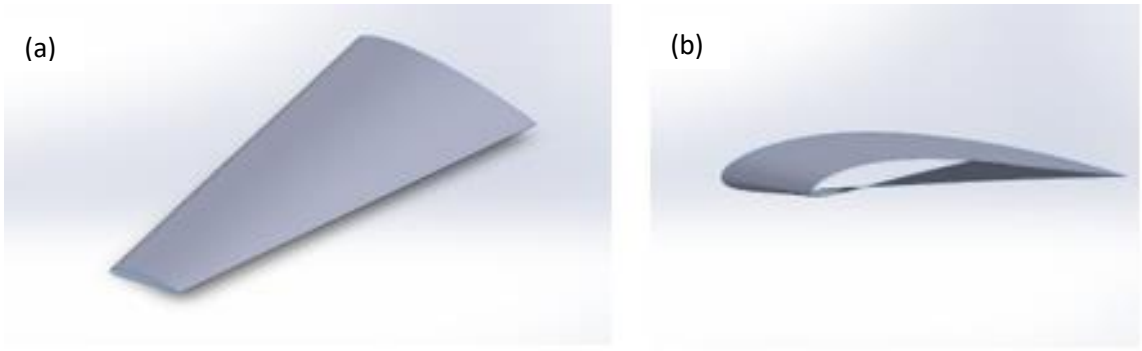

Fig. 6. Wing geometry: (a) top view, and (b) side view

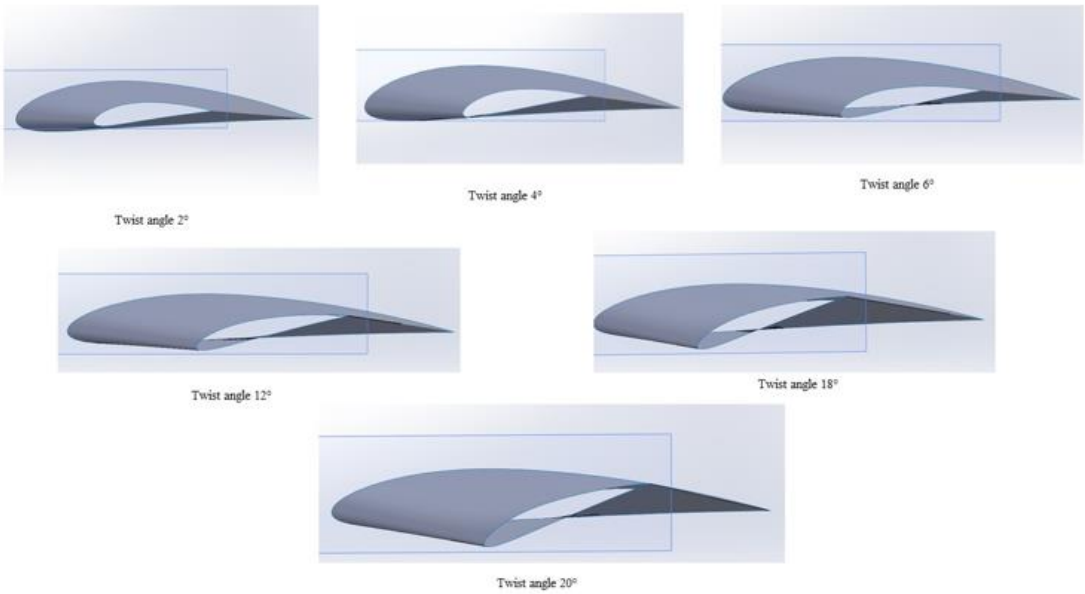

Fig. 7. Wing geometry for different twist angles

2.3.2.2 Computational Domain for 3D Wing

The rectangular computational domain is created in Figure 8. The dimension of the upstream side is 4C, and the downstream side is 6C. The vertical sides of both parts are kept at 2C. The body of influence is also created to analyze the wake region of the wing properly.

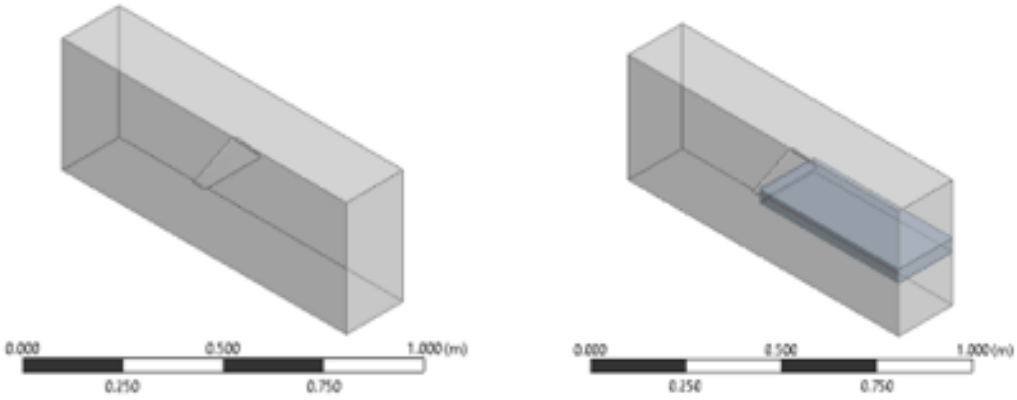

(a) (b)

Fig. 8. Computational domain for 3D wing

2.3.2.3 Grid Generation and Wall Treatment for 3D Wing

The analysis region must be divided into several subregions to apply the finite volume method. These small areas are elements that are joined together at close nodes. The geometric qualities of the generated elements influence the finite volume analysis's overall efficacy and correctness. As a result, mesh fabrication is one of the most important phases in finite-volume modeling.

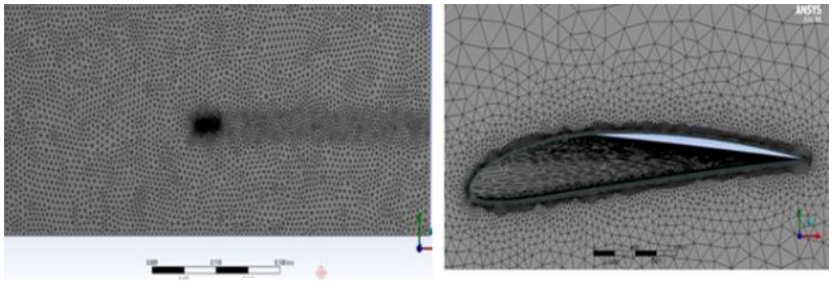

(a) (b)

Fig.9. Mesh around a 3D wing, (a) zoom-out view, and (b) zoom-in view

From Figure 9, we can see flow domains are subdivided into more manageable subdomains to study fluid flow. Each of these subdomains is then used to discretize and solve the governing equations.

A quadrilaterals-method rectangular-type mesh is used to discretize the wing's flow field. 910887 elements and 270192 nodes make up the grid. Inflation and the body of influence approach are utilized to provide precise results in the vicinity of the wake and wing regions.

2.3.2.4 Boundary Condition for 3D Wing

According to Figure 10, the downstream vertical line is the pressure outlet, the two outer horizontal lines are the pressure far field, and the upstream half of the rectangle is the velocity intake.

Here, the inlet section's velocity is 50 m/s. The outlet's atmospheric pressure is measured. Far-field pressure is constant. Turbulence intensity is also taken into account for the velocity inlet boundary condition at 1% and the pressure outlet boundary condition at 5%. A turbulence viscosity ratio of 10 is also employed for a better approximation.

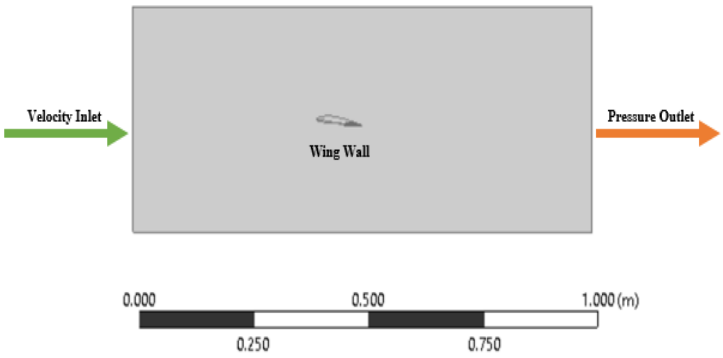

Fig.10. Boundary conditions for 3D wing

3.0 Results and Discussion

Simulations for various angles of attack and Reynolds numbers were run to ascertain the performance of the airfoils. Simulations were carried out specifically for low wind operations and, as a result, for low Reynolds numbers. Various AOAs ranging from -50 to 200 are used to solve the models. Additionally, computational analyses of various wing designs were carried out to identify the ideal twist angle.

3.1 Mesh dependency test

As we can see from Table 1, the drag and lift coefficients on the flow field exhibit identical magnitudes for elements with numbers 160000 and 32000. Consequently, the domain with 160000 items was selected as a standard domain for the subsequent simulation phase.

Table 1
Table of mesh dependency for 2D airfoil analysis

Mesh Element	Drag Coefficient (C_d)	Lift Coefficient (C_l)
50000	0.018359	0.344398
100000	0.018462	0.344541
160000	0.018466	0.344542
240000	0.018466	0.344542
320000	0.018465	0.344543

Table 2
Table of mesh dependency for 3D wing

Number of Mesh Element	Lift Coefficient (C_l)
500667	0.00849
755789	0.00858
809601	0.00881
910887	0.00896
1022345	0.00897
1204567	0.00897

Table 2 shows that the wing's lift coefficient on the flow field exhibits identical magnitudes for elements with numbers 910887 and 1204567. Consequently, the domain with 910887 items was selected as a standard domain for the subsequent simulation phase.

3.2 Solver set-up validation

When solving the forces on an airfoil, the resultants are typically split into two forces. Lift and drag forces are two parts of the net force that act perpendicular to and normal to the incoming flow stream. For various AOA computed with SST (*k*–ω) turbulence models, the lift and drag coefficient graph is displayed and contrasted with confirmed data in Figures 11 and 12.

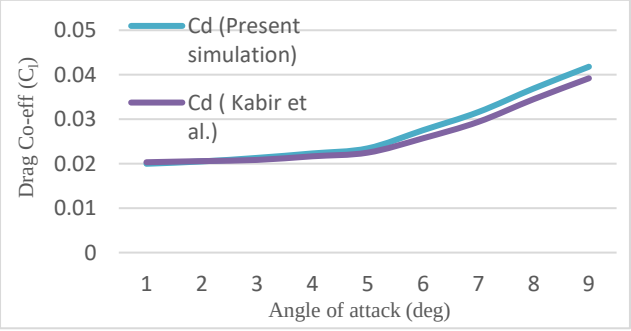

Fig. 11. C_d vs AOA for numerical result and reference work for NACA 4415 [11]

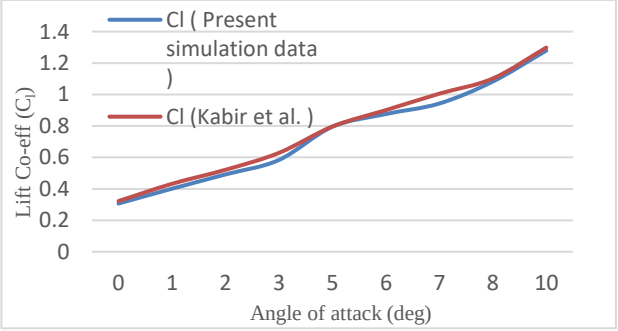

Fig. 12. C_l vs AOA for numerical result and reference work for NACA 4415 [11]

3.3 Observation of Drag and Lift Co-efficient

3.3.1 Observation of Drag and Lift Co-efficient for NACA 4412 and NACA 4418

From Figure 13, it can be seen that at high Reynolds numbers both the airfoil's drag coefficient is closely the same but in lower Reynolds number drag is much higher in NACA 4418 airfoil than NACA 4412. An airfoil's drag will often be higher for thicker airfoils than for thinner ones. This is due to the increased cross-sectional area of a thicker airfoil, which will produce more pressure drag. However, an airfoil's drag characteristics are also significantly influenced by where the greatest camber is. For NACA 4412 and NACA 4418, the maximum camber for NACA 4412 is at 40% of the chord length, whereas the maximum camber for NACA 4418 is at 50% of the chord length. In comparison to NACA 4418, NACA 4412 has a narrower leading edge and a more progressive curve. The more gradual curvature of the airfoil means that the airflow can remain attached to the surface of the airfoil for a longer distance, which results in lower pressure drag.

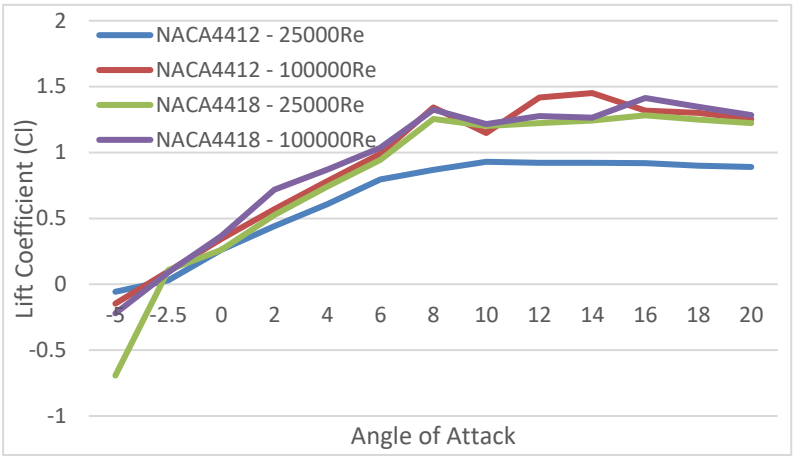

Fig. 13. Numerical data for a drag coefficient of NACA 4412 and NACA 4418 for Reynolds number =25000 & 100000

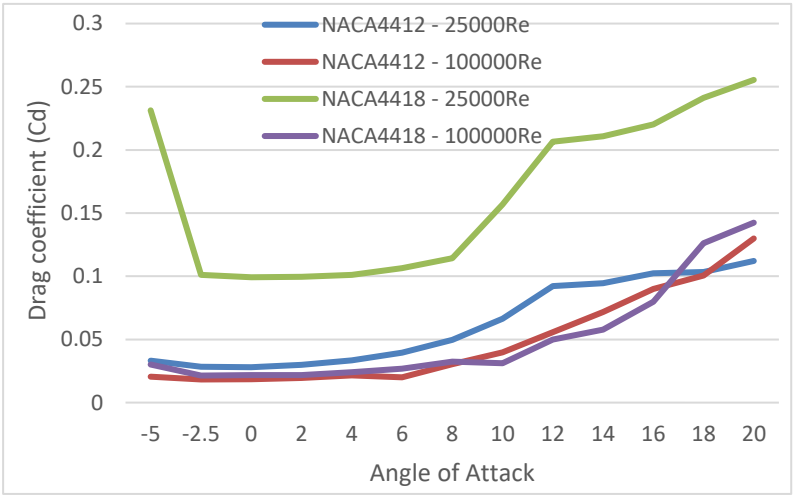

Fig.14. Numerical data for lift coefficient of NACA 4412 and NACA 4418 for Reynolds number = 25000 & 100000

The features of each airfoil's lift curve should be taken into account while contrasting the lift characteristics of the NACA 4412 and NACA 4418 airfoils. In Figure 14, The link between the AOA (the angle between the airfoil and the entering air) and lift coefficient is shown by the lift curve of an airfoil (the amount of lift generated by the airfoil). The change in lift coefficient for a specific change in angle of attack is measured by the lift curve slope. In comparison to the NACA 4418 airfoil, the NACA 4412 airfoil typically has a higher maximum lift coefficient and a steeper lift curve slope. As a result, at smaller angles of attack, the NACA 4412 airfoil can provide more lift than the NACA 4418 airfoil. The NACA 4412 airfoil, has a larger maximum lift coefficient, which may be advantageous for producing high power at higher wind speeds.

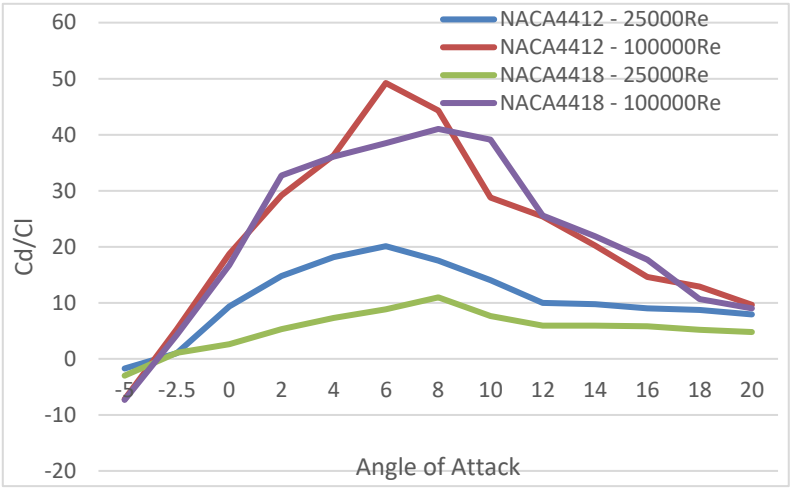

Fig. 15. Lift-to-drag ratio vs AOA for NACA 4412 and 4418 for Reynolds number =25000 &100000

The NACA 4412 airfoil typically has a lower drag coefficient at low to medium angles of attack, which can be advantageous for lowering drag. For wings at greater angles of attack, the NACA 4418 airfoil provides a reduced drag coefficient at high angles of attack.

Although both airfoils are capable of producing high lift coefficients, the ideal angle of attack for maximizing the lift-to-drag ratio will vary depending on the particular operating circumstances of the wind turbine. A higher lift-to-drag ratio, which means the airfoil produces more lift for a given amount of drag, often denotes a more efficient airfoil.

The NACA 4418 airfoil retains lift at higher angles of attack at low speeds, which is advantageous for low-wind operation. In comparison to the NACA 4412 airfoil, which has not maintained lift as effectively at higher angles of attack, this can lead to a higher lift-to-drag ratio at lower wind speeds. But NACA 4418 also has a higher drag coefficient which means it will face more drag as well due to its thicker profile.

The NACA 4412 airfoil has a higher maximum lift coefficient and a steeper lift curve slope than the NACA 4418 airfoil, making it appropriate to use at high speeds. At higher wind speeds, where greater lift coefficients are needed, it can lead to a larger lift-to-drag ratio. From the Figure 15, it is seen that NACA 4412 is producing a higher lift-to-drag co-efficient ratio even is a low Reynolds number.

3.3.2 Observation of Lift and Drag Co-efficient for 3D Wing

A wing's lift coefficient quantifies how much lift the wing produces at a specific angle of approach. The angle between the wing's base and tip is referred to as the twist angle. As the twist angle increases, the wing sections' angle of attack toward the wing's tip decreases, which lowers the quantity of lift produced by these sections. The quantity of lift produced by the wing sections is increased concurrently with an increase in the wing sections' angle of attack towards the wing's root.

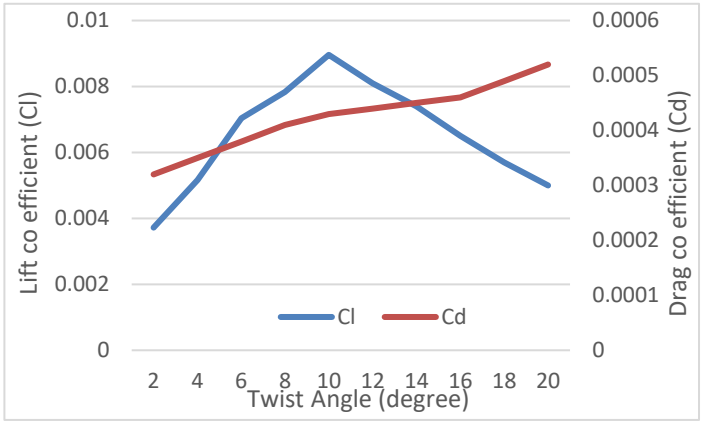

Fig. 16. Lift co-efficient and drag co-efficient Vs twist angle graph for the wing

From Figure 16, it can be seen that *Cl* rises with the increase in the twist angle of the wing initially. But then it goes downward. A very high twist angle can separate the flow and raise the drag, reducing the lift coefficient. The lift coefficient may also achieve a maximum value at high angles of attack before beginning to decline as the angle of attack is raised even higher.

It has been observed that raising a wing's twist angle causes the drag coefficient to rise. This is because a large twist angle can make flow separation happen early and more abruptly along the wing, expanding the turbulent wake's size and increasing wing drag.

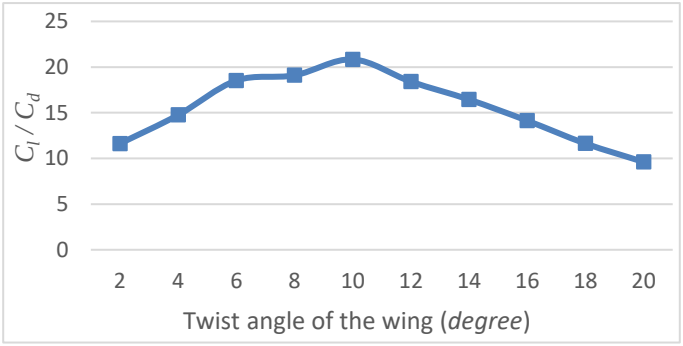

Fig. 17. Lift-to-drag ratio vs. Twist angle curve for wing

The effectiveness of a wing in producing lift while creating the least amount of drag is indicated by the lift-to-drag ratio of the wing. Here, in Figure 17, Cl/Cd initially rises with the twist angle and begins to fall after reaching an optimal value.

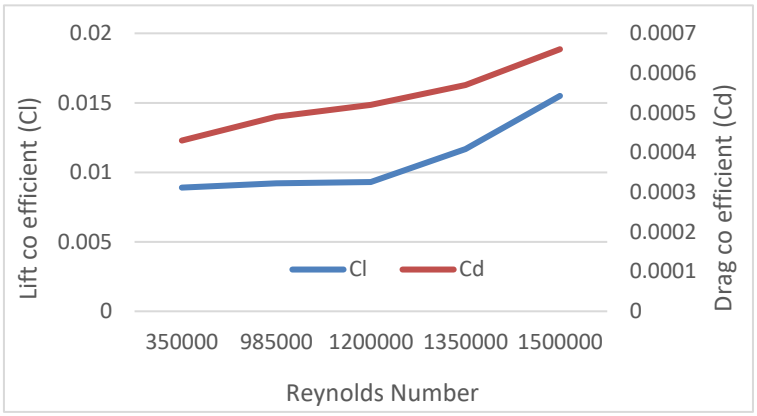

Fig. 18. Lift coefficient and drag co-efficient Vs Reynolds number curve for wing

The Reynolds number significantly influences the lift coefficient, which is proportionate to the ratio of the fluid's inertial forces to its viscous forces. Figure 18 shows that viscous forces dominate the flow around the wing at lower Reynolds numbers, and the lift coefficient is comparatively low. The inertial forces, however, become more powerful as the Reynolds number rises, increasing the lift coefficient.

Similar to how the Reynolds number impacts the lift coefficient, the flow around the wing affects the drag coefficient. Figure 18 shows that lower Reynolds numbers result in a comparatively low drag coefficient. However, as the Reynolds number rises, the movement becomes more turbulent, causing the drag coefficient to rise.

3.4.1 Static Pressure Contours for NACA 4412

When analyzing the behavior of the air around an aerodynamic object, such as an aircraft, wing, missile, or vehicle, static pressure is crucial. The lift and drag forces acting on an object's surface are influenced by changes in static pressure, which also has an impact on the object's overall aerodynamic performance. In the accompanying Figure 19, the flow is symmetrical around the airfoil, and the static pressure is constant at zero angle of attack. The flow separates from the airfoil's upper surface as the angle of attack rises, resulting in a region of low static pressure. This area, which is at the airfoil's leading edge, is referred to as the "upper surface suction peak" or "leading-edge suction peak."

The low-pressure area expands in size as the angle of attack rises, and a separation point develops on the upper surface of the airfoil. A sharp decrease in lift and a significant rise in drag at this separation point indicate the start of the stall.

As can be seen in the picture, the static pressure contours over an airfoil are not symmetrical for the top and lower surfaces at a 0° angle of attack. As a result, at a 0° angle of attack, there is some lift. At a 6° angle of attack, an area of low pressure on the airfoil's upper surface causes the flow to stall just beneath the leading edge and produce lift. The low-pressure area moves forward while the high-pressure area moves with an increasing attack angle toward the airfoil's bottom surface.

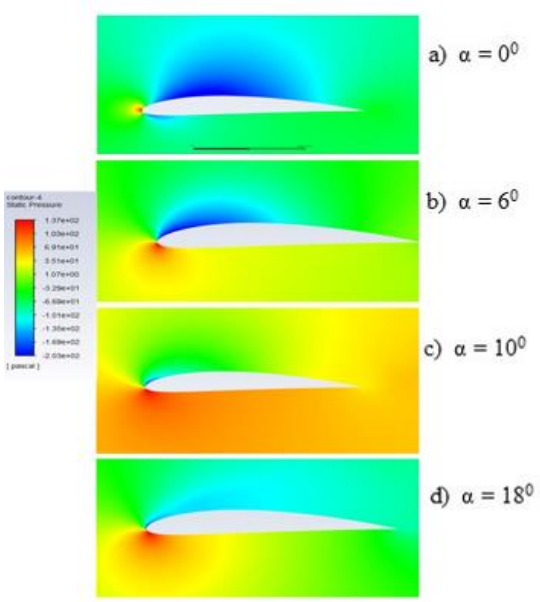

Fig. 19. Static pressure contours of NACA 4412 for different angles of attack

3.4.2 Static Pressure Contours for NACA 4418

Figure 20 shows that the NACA 4418 airfoil's upper surface has higher static pressure than its lower surface and that the dynamic pressure increases as air velocity increases.

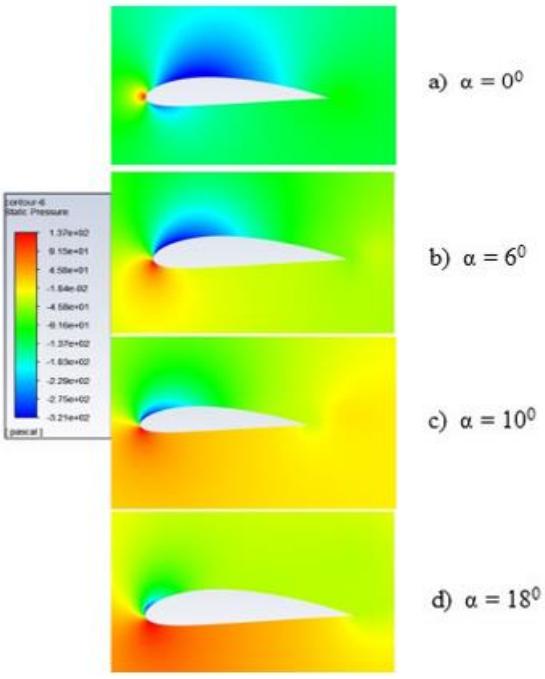

Fig. 20. Static pressure contours of NACA 4418 for different angles of attack

The angle of attack, which is the angle created by the chord line of the airfoil and the incoming airflow, is observed to have an impact on the static pressure distribution on the surface of the NACA 4418 airfoil. When the angle of attack is zero, the static pressure on the top and bottom surfaces of

the airfoil are almost equal at the leading point. The pressure on the lower surface of the airfoil grows as the angle of attack rises, creating a net upward force or lift.

3.5 Static pressure contours for the wing

Figure 21 shows that a shift in the static pressure distribution along a wing's surface results from increasing the twist angle of the wing. This is so because the twist angle impacts local airflow and pressure distribution, which also affects the angle of attack of the wing sections across the span of the wing. Depending on the particular wing design and the operational circumstances, the overall impact of these variations in pressure distribution may differ. Increasing the twist angle can generally result in a more even spread of lift across the wing's span, but it can also increase drag, especially in places where the flow separates from the wing's surface.

The optimal twist angle for the wing is 10°. For this geometry of the wing, the maximum lift coefficient to drag co-efficient ratio, which is 20.83, is determined.

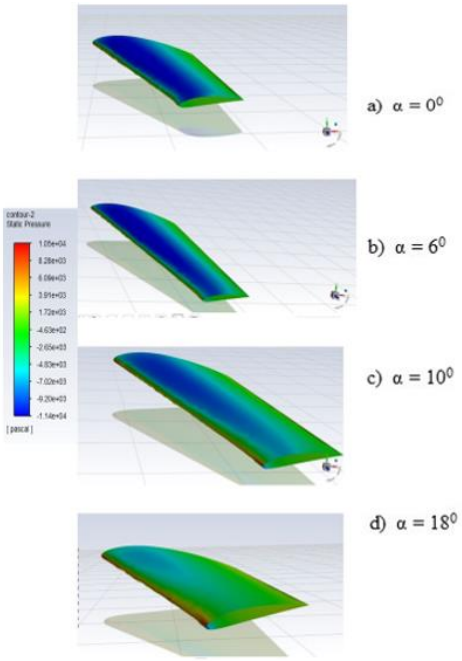

Fig. 21. Static pressure contours for wing

4. Conclusions

In this research, firstly, the performance parameters of airfoils NACA 4412 and NACA 4418 has been analyzed and compared using different angle of attack by 2D CFD analysis, and secondly, the aerodynamic properties of a wing have been numerically investigated for varying Reynolds number as well as the optimal twist angle of the wing geometry has been analyzed using 3D CFD analysis. The Reynolds average Navier-Strokes equation has been solved numerically to determine the flow properties applying the SST k−ω turbulence model as the viscous modeling in the computational solver. Validation of the numerical data was also compared with the reference work data. From the result and discussion, it is clear that for both low and high Reynolds numbers, the NACA 4412 is the better performer as it has a higher lift-to-drag ratio in both cases. For NACA 4412 maximum lift-to-drag coefficient ratio is 49.22 for a 6-degree angle of attack at the Re=100000, and for NACA 4418, it is 41.23 at the 8-degree angle of attack. For Re=25000, NACA 4412 gives a maximum lift coefficient

to drag coefficient ratio is 20.10, also for a 6-degree angle of attack, whereas for NACA 4418, it is 10.97 for an 8-degree angle of attack. On the other hand, the wing's lift coefficient is significantly influenced by the Reynolds number. At first, the lift coefficient increases slowly with Re, but it rises sharply from Re=1200000, which means the lift coefficient significantly rises with the flow velocity. The drag coefficient also increases with the Reynolds number due to a rise in turbulence. However, with a twist angle, the lift coefficient increases to a certain point, after which it decreases with the increase of the twist angle, but the drag coefficient always rises with the twist angle. The optimum twist angle for the wing is 10°, and from this angle, we get the maximum lift-to-drag coefficient ratio of 20.83. In the future, this study can be further optimized by testing it in unsteady states, and different types of high-lift devices, such as flaps and leading edge slats, can be used on the airfoil to increase the lift.

Acknowledgment
The authors are grateful for the facilities and financial support from Khulna University of Engineering & Technology.

References

[1] Sobieczky, H., "Parametric Airfoils and Wings," In Notes on Numerical Fluid Mechanics, (1999): 71–87. https://doi.org/10.1007/978-3-322-89952-1_4.
[2] Triet, Nguyen Minh, Nguyễn Ngọc Việt and Pham Manh Thang, "Aerodynamic Analysis of Aircraft Wing," VNU Journal of Science: Mathematics-Physics 31, no. 2 (2015). https://js.vnu.edu.vn/index.php/MaP/article/download/111/105
[3] James, R.M., "The Theory and Design of Two-Airfoil Lifting Systems," Computer Methods in Applied Mechanics and Engineering 10, no. 1 (1977): 13-43. https://doi.org/10.1016/0045-7825(77)90032-9
[4] Tay, Wee Beng, "Effect of Different Types of Wing-Wing Interactions in Flapping MAVs," Journal of Bionic Engineering 14, no. 1 (2017): 60-74. https://doi.org/10.1016/S1672-6529(16)60378-5
[5] Devinant, Philippe, Thomas Laverne and J Hureau, "Experimental Study of Wind-Turbine Airfoil Aerodynamics in High Turbulence," Journal of Wind Engineering and Industrial Aerodynamics 90, no. 6 (2002): 689–707. https://doi.org/10.1016/S0167-6105(02)00162-9
[6] Tao, Siyu, Daniel W. Apley, Wei Chen, Andrea Garbo, David J. Pate and Brian J. German, "Input Mapping for Model Calibration with Application to Wing Aerodynamics," AIAA Journal 57, no. 7 (2019): 2734-2745. https://doi.org/10.2514/1.J057711
[7] Camacho, Emanuel A., André R. Silva and Flávio D. Marques, "Optimal Operation of the NACA0012-IK30 Airfoil," *AIAA AVIATION 2023 Forum*, June (2023): 4439. https://doi.org/10.2514/6.2023-4439
[8] Cayiroglu, Ibrahim and Recep Kiliç, "Wing Aerodynamic Optimization by Using Genetic Algoritm and Ansys," Acta Physica Polonica A 132, (2017): 981-985. 10.12693/APhysPolA.132.981
[9] Ives, Rob, (Andrew) Stewart KEIR, Edet Bassey and Faik A. Hamad, "Investigation of the Flow Around an Aircraft Wing of Section NACA 2412 Utilizing ANSYS fluent," *INCAS Bulletin* 10, no. 1 (2018).
[10] Zilstra, Alison and David A. Johnson, "Large Eddy Simulation of Transitional Separated Flow Over a Low Reynolds Number Cambered Airfoil," Journal of Fluids Engineering 145, no. 3 (2023): 031303. https://doi.org/10.1115/1.4056280
[11] Kabir, Asif, Yeasir Mohammad Akib, Mahdi Hasan and Md Jahirul Islam, "Comparison of the Aerodynamic Performance of NACA 4415 and KFm Based Stepped Airfoils," *AIP Conference Proceedings* 2324, no. 1 (2021): 040003. https://doi.org/10.1063/5.0037582
[12] Srinivasan, G.R. and Wil J. McCroskey, "Navier-Stokes Calculations of Hovering Rotor Flowfields," Journal of Aircraft 25, no. 10 (1988): 865-874. https://doi.org/10.2514/3.45673

[13] Devinant, Ph., T. Laverne and J. Hureau, "Experimental Study of Wind-Turbine Airfoil Aerodynamics in High Turbulence," Journal of Wind Engineering and Industrial Aerodynamics 90, no. 6 (2002): 689-707. https://doi.org/10.1016/S0167-6105(02)00162-9
[14] Menter, F.R., "Two-Equation Eddy-Viscosity Turbulence Models for Engineering Applications," *AIAA Journal* 32, no. 8 (1994): 1598-1605. https://doi.org/10.2514/3.12149
[15] Menter, F.R., "Zonal Two Equation k-ω Turbulence Models for Aerodynamic Flows," *23rd Fluid Dynamics, Plasmadynamics, and Lasers Conference*, (Orlando,FL,USA: Aerospace Research Central, 6-9 July, 1993). https://doi.org/10.2514/6.1993-2906
[16] NACA 4 Digit Airfoil Database Search." n.d. http://airfoiltools.com/search/index?m%5Bgrp%5D=naca4d&m%5Bsort%5D=1